VOL. 18, NO. 8, APRIL 2023 ISSN 1819-6608
ARPN Journal of Engineering and Applied Sciences

www.arpnjournals.com

CLASSIFICATION OF OBJECTS WITHIN AGRICULTURAL LANDSCAPE FROM HIGH-RESOLUTION AERIAL IMAGERY USING MAXIMUM LIKELIHOOD DISCRIMINANT RULES

Asmala Ahmad[1], Mohd Yazid Abu Sari[2], Hamzah Sakidin[3], Suliadi Firdaus Sufahani[4], Abd Rahman Mat Amin[5] and Abd Wahid Rasib[6]

[1]OptiMAS Research Group, Centre for Advanced Computing Technology (C-ACT), Faculty of Information and Communication Technology, Universiti Teknikal Malaysia Melaka, Hang Tuah Jaya, Durian Tunggal, Melaka, Malaysia
[2]Anjung Technology Sdn. Bhd., Ayer Keroh, Melaka, Malaysia
[3]Department of Fundamental and Applied Sciences, Universiti Teknologi PETRONAS, Perak, Malaysia
[4]Fakulti Sains Gunaan dan Teknologi, Universiti Tun Hussein Onn Malaysia, Parit Raja, Batu Pahat, Johor, Malaysia
[5]Fakulti Sains Gunaan, Universiti Teknologi MARA Cawangan Terengganu, Kuala Terengganu, Terengganu, Malaysia
[6]Fakulti Alam Bina DanUkur, Universiti Teknologi Malaysia, UTM Skudai, Johor, Malaysia
E-Mail: asmala@utem.edu.my

ABSTRACT

In this study, the performance of object classification based on four discriminant functions, namely linear, quadratic, diagonal linear and diagonal quadratic is investigated and compared. High-resolution aerial imagery captured from a UAV-based remote sensing platform is used for this purpose. Initially, K-means clustering of 9 clusters is used to assist in the selection of training pixels for the subsequent supervised classification implementation. The classification is experimented with using a training set size of 10 through 100 pixels for each of the discriminant functions. The outcome of the classification shows that training set size 40 and 10 are to be the optimal training set sizes for linear and quadratic discriminant function, and diagonal linear and quadratic discriminant function respectively. Overall, the linear discriminant function is found to have the highest overall accuracy of 91% followed by diagonal linear, quadratic, and diagonal quadratic discriminant function with overall accuracies of 82%, 79%, and 73% respectively.

Keywords: classification, accuracy, training set size, discriminant function, paddy.

Manuscript Received 20 January 2023; Revised 23 May 2023; Published 15 June 2023

INTRODUCTION

The world population is predicted to grow alarmingly from 7.8 billion in 2020 to 8.3 billion in 2030 and to 9.1 billion in 2050 where food demand is predicted to increase by 40% and 60% respectively. This leads to the need to ensure 40% - 60% more food is secured in 10 - 30 years. A way to do this is to increase crop production by systematically managing crop growth. This is important especially for paddy which serves as the staple food for 3.5 billion people, including Malaysians, in which are nearly 50% of the world's population [1]. In 2019, Paddy has been planted around 12% of the world's total agricultural land with approximately 167.3 million hectares [2]. On average, the rice production from paddy plantations in Malaysia is only 2.5 metric tons per hectare and is among the lowest in the Southeast Asia region. This is due to the issues in paddy management and external factors such as disease and disaster attacks. Although the world's paddy cultivation areas have increased from year to year in many countries, nevertheless, rice demands still exceed their yield production [3]. In recent decades, two main issues, namely the increase in the world population (especially in the countries where rice has been the main staple food) and climate change have triggered an awareness of how rice production will always be sufficient to accommodate the demand. It has been years that Malaysian rice production has experienced 30% shortage than consumption and therefore is dependent on rice import from other Southeast Asia countries [4].

Therefore, numerous efforts have been carried out to maintain and increase rice production in which the most popular one is known as precision agriculture [2]. Precision Agriculture can be defined as a method to increase the effectiveness of agricultural management to maximise food production. Precision agriculture also refers to a holistic crop management by means of optimising the use of resources (right amount of input). This is to maximise the results (yield), at the right time and at the right place, also known as the concept of 3R aiming to increase crop yield without neglecting environmental protection.

To meet such a definition, remote sensing technology has long been used to monitor crop status [3]. Initially, in the 1980s, satellite remote sensing technology has started to be used in monitoring various crops to fulfil the needs of precision agriculture due to its capability to capture images of large-scale agricultural land continuously with cheaper costs compared to traditional approaches. Among the frequently used remote sensing satellites include Landsat, SPOT, IKONOS and Quick bird. Nevertheless, satellite imagery is exposed to other crucial issues especially cloud and haze effects which lead to loss of surface information [5]. Satellite systems are operated by satellite operators in developed countries in which users do not have any autonomy over them. Most

critical of all, satellite images also suffer limitations in terms of spatial and temporal resolution [7] particularly for small-sized crops such as paddy.

To overcome such problems, we have developed a technique for object recognition known as Personal Remote Sensing System (PRSS) [6]. The technique involves pre-set autonomous UAV navigation and utilizes RGB spectral bands with high spatial resolution enabling monitoring of agricultural crops to be done systematically with desired spectral, spatial and temporal resolution. Effort on UAV-based applications on paddy via classification has been recently carried out using a number of unsupervised classifiers [36] however, due to the very high spatial resolution of the UAV imagery, paddy can easily be misclassified as weeds due to the similarity in statistical properties of the pixels' reflectance from these plants. There has also been an effort of using supervised classifiers [37] where higher classification accuracy was able to be achieved; nevertheless, the major barrier is the difficulty in identifying the correct training pixels. Moreover, the accuracy of supervised classification is very much dependent on the correctness of the training pixels used. So far, most published articles on paddy classification using UAV-based imagery have applied a single classification scheme although each has limitations. Studies have shown that hybrid classification by combining unsupervised and supervised classifiers [1], [8], [9], [10] produced promising results when using satellite images but not much is known if these are to be applied on UAV-based imagery. This work reported in this article utilises unsupervised and supervised classifiers on UAV-based imagery of agricultural landscape, with paddy as the main crop, based on linear, quadratic, diagonal linear and diagonal quadratic discriminant function.

CLASSIFICATION

In remote sensing, classification is the process of assigning a pixel to a particular type of object. Classification uses typically a measurement vector or feature vector ω of data acquired from a space borne or airborne acquisition system. Its purpose is to assign a pixel associated with the measurement ωat position **x** to particular class i, where $1 \leq i \leq M$ and M is the total number of classes. The classes are defined from supporting data, such as maps and ground data for test sites. Two types of classification are commonly used, unsupervised and supervised.

Unsupervised classification is a two-step operation of grouping pixels into clusters based on the statistical properties of the measurements. This is followed by labelling the clusters with the appropriate classes. The clustering process produces clusters that are statistically separable, giving a natural grouping of the pixels [10]. Frequently used unsupervised classification is K-means and ISODATA.

On the other hand, supervised classification starts from a known set of classes. A chosen supervised classifier learns the statistical properties of each class and then assigns the pixels based on these properties. Supervised classification classifies pixels based on known properties of each object type; it requires representative object information, in the form of training pixels [1], [8], [9]. Signatures generated from the training pixels will be in a different form, depending on the classifier type used. Examples of supervised classification classifiers include Naïve Bayes, Maximum Likelihood, Mahalanobis Distance, Parallelepiped and support vector machines.

The implementation of unsupervised classification is simpler and more straightforward compared to supervised classification however it may happen that more than one generated clusters are belonging to the same class due to the fact that such classification depends merely on the statistical properties of the pixels. On the contrary, supervised classification has been regarded as a more robust and stable method compared to the unsupervised classification due to the use of training pixels in generating a signature for each of the land covers. Nevertheless, the performance of supervised classification depends very much on the correctness of the training pixels selection which is frequently done manually and therefore exposed to human errors.

K-means Clustering

K-Means algorithm is an iterative method to partition a given dataset into a user-specified number of clusters, k. i is the cluster number, **n** is the number of data points with the same cluster centre, and **j** denotes the jth pixel with the same cluster centre [10], [11]. The main goal of K-Means is to minimize the sum of squared error among data points and their respective cluster centres. Let $\boldsymbol{\mu_c}$ denotes the mean for cluster centre **c**, and the K-Means objective function can be written as:

$$J(c, \mu) = \sum_{i=1}^{k} \sum_{j=1}^{n} \|x_i - \mu_c\|^2 \quad (1)$$

Where, **J** measures the sum of squared distances between each data point **x** and the cluster centroid $\boldsymbol{\mu_c}$to which it has been assigned. The inner-loop of K-Means repeatedly minimizes **J** with respect to **c** while holding **μ** fixed, and then minimizes **J** with respect to **μ** while holding **c** fixed. With this function well defined, the process can be split into several steps, to achieve the intended result.

Maximum Likelihood Discriminant Rules

In supervised classification, the object conditional densities $P(\boldsymbol{\omega}|i = k)$are known [12], [13] where i is the class label while k is the object class. The maximum likelihood (ML) discriminant rule predicts the class of an object based on the feature vector $\boldsymbol{\omega} = \omega_1, \omega_2, \ldots, \omega_p$, where p is the number of spectral measurement (the number of spectral bands used). In practice, the parameters are estimated from a training set. Using parameter estimates in place of the unknown parameters yields the ML discriminant rules [14], [16]. For multivariate normal class densities, that is, for $\boldsymbol{\omega}|i = k \sim N(\mu_k, C_k)$. Four types of rules can be considered [12]:

a) Quadratic discriminant analysis (QDA) where the discriminant rule is:

$$\hat{\mathbf{i}} = \text{argmin}_k\{(\boldsymbol{\omega} - \mu_k)\sum_k^{-1}(\boldsymbol{\omega} - \mu_k)' + \log|C_k|\} \quad (2)$$

where k is the class label. This is also known as the general form of the rule.

b) Linear discriminant analysis (LDA). For this case, the class densities have the same covariance matrix $C_k = C$, the discriminant rule is based on the square distance and is linear in **i**, and given by:

$$\hat{\mathbf{i}} = \text{argmin}_k\{(\boldsymbol{\omega} - \mu_k)\sum^{-1}(\boldsymbol{\omega} - \mu_k)'\} \quad (3)$$

c) Diagonal quadratic discriminant analysis (DQDA). For this case, the class densities have a diagonal covariance matrix, $\Delta_k = \text{diag}(\sigma_{k1}^2, \ldots, \sigma_{kp}^2)$, the discriminant rule is given by additive contributions from each object:

$$\hat{\mathbf{i}} = \text{argmin}_k \sum_{j=1}^{p}\left\{\frac{(\omega_j - \mu_k)^2}{\sigma_k^2} + \log\sigma_k^2\right\} \quad (4)$$

d) Diagonal linear discriminant analysis (DLDA). For this case, when the class densities have the same diagonal covariance matrix $\Delta = \text{diag}(\sigma_k^2, \ldots, \sigma_p^2)$, the discriminant rule is linear and given by:

$$\hat{\mathbf{i}} = \text{argmin}_k \sum_{j=1}^{p}\left\{\frac{(\omega_j - \mu_{kj})^2}{\sigma_k^2}\right\} \quad (5)$$

Classification Accuracy

A confusion matrix is frequently used in determining classification accuracy and it works by comparing classification result with reference information. Accuracy is conveyed in terms of percentage of overall classification accuracy and producer accuracy [30], [31]. Producer accuracy is a measure of the accuracy of a particular classification scheme and shows the percentage of a particular ground class that has been correctly classified. The minimum acceptable accuracy for a class is 70% [29], [32]. This is calculated by dividing each of the diagonal elements of a confusion matrix by the total of the column in which it occurs:

$$\text{Producer accuracy} = \frac{c_{aa}}{c_{\bullet a}} \quad (6)$$

where,

c_{aa} = element at position a^{th} row and a^{th} column
$c_{\bullet a}$ = column sum

A measure of behaviour of a classification can be determined by the overall accuracy, which is the total percentage of pixels correctly classified:

$$\text{Overall accuracy} = \frac{\sum_{a=1}^{U} c_{aa}}{Q} \quad (7)$$

where Q and U represent the total number of pixels and classes respectively. The minimum acceptable overall accuracy is 85% [34]. The Kappa coefficient κ is a second measure of classification accuracy which incorporates the off-diagonal elements as well as the diagonal terms to give a more robust assessment of accuracy than overall accuracy. This is computed as:

$$\kappa = \frac{\sum_{a=1}^{U}\frac{c_{aa}}{Q} - \sum_{a=1}^{U}\frac{c_{a\bullet}c_{\bullet a}}{Q^2}}{1 - \sum_{a=1}^{U}\frac{c_{a\bullet}c_{\bullet a}}{Q^2}} \quad (8)$$

where $c_{a.}$ is row sum and $c_{.a}$ is column sum and 0.81 can be taken as the minimum acceptable Kappa coefficient.

METHODOLOGY

Image Acquisition

Image acquisition was carried out based on Personal Remote Sensing System or PRSS concept [17], [18]. The PRSS concept has been established in the previous research for overcoming limitations in term of spatial resolution besides cloud and haze [33], [35] effects that degrade space-borne remote sensing satellite imagery [1], [19], [20], [21]. This system consists of 1) aerial segment, 2) ground segment and 3) user segment. The aerial segment consists of a quad rotor UAV that is equipped with GPS and telemetry facilities and mounted with a high-resolution RGB camera [22], [23], [24]. Images are captured automatically at desired time intervals and stored in the camera's storage card. Upon completing an image acquisition mission, images in the card are transferred to the ground segment for subsequent image processing tasks. The ground segment consists of a laptop installed with software for controlling and tracking the UAV besides processing captured images [25]. Processed images are finally uploaded to the cloud-based geospatial databases that can finally be accessed and personalised using a smart phone at the user segment. Figure-1 illustrates the PRSS concept.

The image used in this study was acquired over paddy field area of Kampung Sawah Sagil located in Batu Pahat, Johor, Malaysia on 1st June 2022 at 0940 local time. The UAV was flown at an altitude of 54 m and the sky was clear. The image is in RGB with size of 3648 rows by 5472 columns and the image format is JPG.

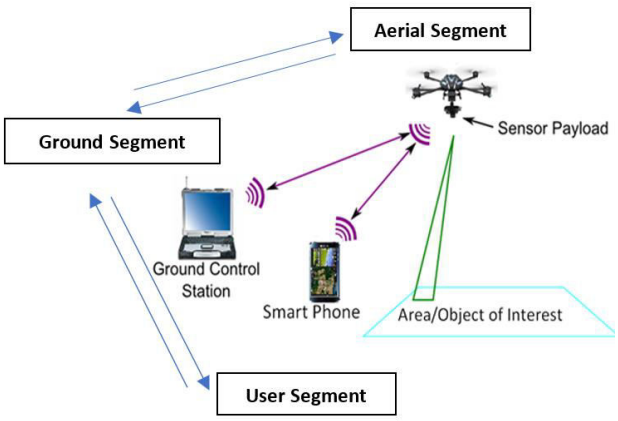

Figure-1. PRSS concept.

Image Classification

The acquired image was initially processed using K-Means clustering algorithm [15]. The K-Means clustered image is to be used together with the existing information of the study area in selecting the training pixels for the subsequent supervised classification. Initially, the number of objects within the study area is assessed through fieldwork visits to the study area. K-means clustering was performed by varying the number of clusters from 1 to 10. Colours were assigned to the clusters randomly. Visual analysis of the K-means clustering outcomes were then performed to determine the number of clusters best match the objects that exist within the study area. The training pixels for each of the classes were then chosen based on the clusters produced by the K-Means clustering besides knowledge of the study area that was gained through the fieldwork visits. After the training pixels have been obtained, we then performed reference pixels collection by making use the same approach. The training pixels were used by the classifier to estimate the mean vector and covariance matrix of each class. Eventually, every pixel in the image is classified into one of the object classes based on four discriminant functions namely linear, quadratic, diagonal linear and diagonal quadratic discriminant function.

Classification Accuracy

One of the most important components in accuracy assessment is reference pixels [26], [27]. In this study, reference pixels were determined based on ground truth knowledge of the study area [28] gained during a number of field visits. In selecting the reference pixels, a systematic sampling is performed where the chosen reference pixels are distributed in a predefined pattern. A confusion or error matrix is then used to analyze the agreement between the training and reference pixels [29].

RESULTS

Figure-2 shows the study area displayed in RGB; it is obvious that the study area has two main groups of objects which are vegetations and non-vegetations. By integrating ground-truth information and visual image analysis, it is clear that paddy fields cover most of the left region of the image is to be the most dominant object. Banana trees can be seen on the top right of the image. There is also a strip of coconut trees scattered approximately in the middle of the image. There are bare ground regions on the middle right and ranging from top to bottom in middle of the image. The latter is an unpaved road in between the paddy fields and a farmer's house yard. The rooftops of the houses are in white and brown colour in which the latter is due to corroded rooftop made from zinc. A strip of bushes can be seen along the right of the unpaved road. Grassy ground can be seen on the top right of the image. On the top middle of the image, there is a water body of an irrigation system to water the paddy fields. Therefore, the classes considered in this study were white rooftop, corroded rooftop, bare ground, grassy ground, bushes, banana, coconut, paddy and water. The image used in this study consists of 3648 rows by 5472 columns equivalent to 1, 996, 2000 pixels that represent 3584 m^2 of actual size. With 54 m flight height, a ground sampling distance (GSD) of 1.3 cm per pixel was able to be achieved. The summary of the image properties shown in Figure-2 are shown in Table-1.

Figure-2. The agriculture landscape under study in RGB image.

Table-1. The properties of the image.

Image width (num. of columns)	**5472 pixels**
Image height (num. of rows)	3648 pixels
Sensor width	13.2 mm
Sensor height	8.8 mm
Focal length	10 mm
Flight height	54 m
Ground sampling dist. (GSD)	1.3 cm/pixels
Image size	19962000 pixels
Actual ground size	3584 m^2

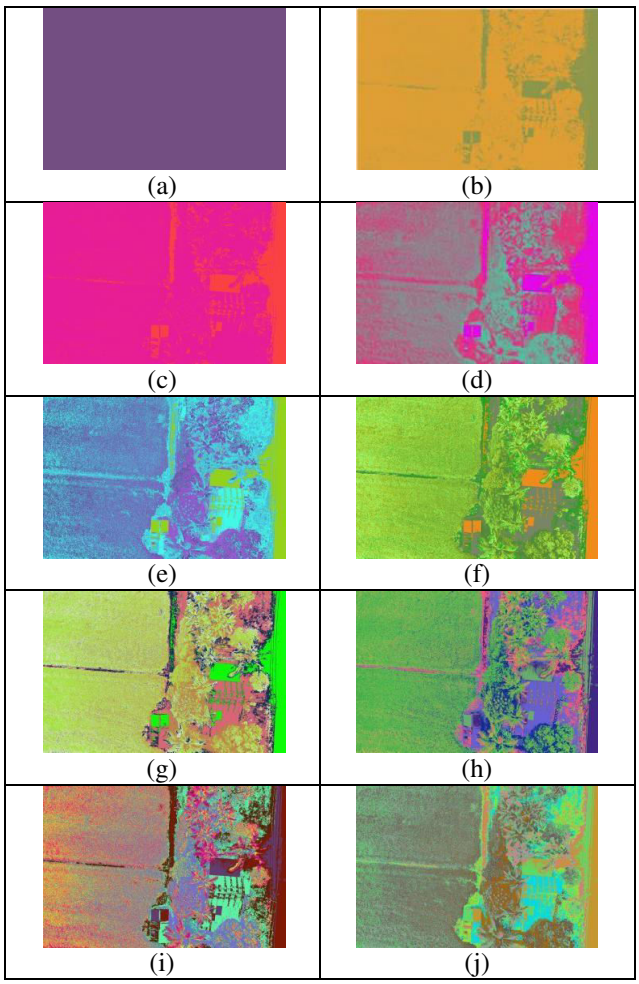

Figure-3. Cluster images produced using K-Means clustering for 1 to 10 clusters (a to h).

Figure-3 shows the result of K-Means clustering that produces 1 to 10 clusters (a to h). Initially, for 1 cluster, the whole image is grouped into a single cluster. For 2 and 3 clusters, vegetation and non-vegetation pixels start to separate apart. For 4, 5 and 6 clusters, different vegetation pixels are grouped into different clusters; the same goes with non-vegetation pixels. For 7 and 8 clusters, separation between bare ground and grassy ground becomes more obvious. For 9 and 10 clusters, more Paddy clusters exist as can be seen from the colour variability within the Paddy field. K-Means clustered image with 9 clusters is found the most sensible to represent the study area and is used to assist the selection of training pixels for the supervised classification. In doing so, both the RGB and K-Means clustered image are displayed side by side and zoomed at the targeted objects. This has provided a practically way for the spatial and spectral homogeneity criteria of training pixels for a particular object to be met [15].

Classification using Linear Discriminant Function

Figure-4 shows plots of overall classification accuracy (top) and Kappa coefficient (bottom) versus training set size for the supervised classification that is based on linear discriminant analysis. It can be seen that the40-training set size gives the overall classification accuracy (91%) and Kappa coefficient (0.9). Plots of classification accuracy (producer accuracy) versus training set for each of the classes are shown in Figure-5. White rooftop and corroded rooftop have the highest (100%) and most stable accuracies for all training pixel sets while the least stable classes are banana, paddy and coconut. This is due to the facts that stable classes have more abundant homogeneous pixels compared to least stable classes. For the rest of the classes, generally high classification accuracies are gained at smaller compared to bigger training set sizes.

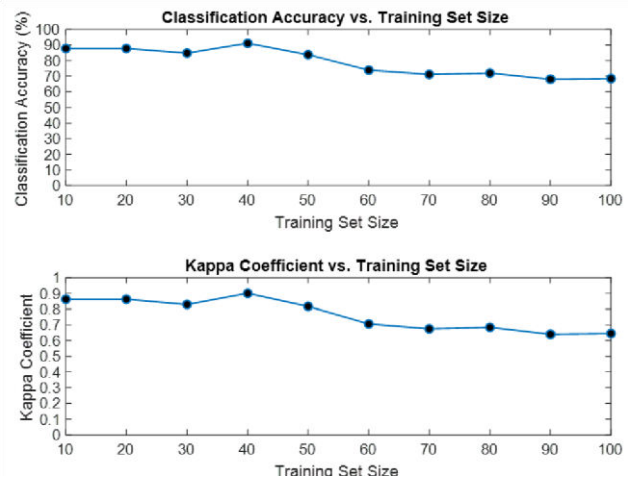

Figure-4. Overall classification accuracy and Kappa coefficient versus training set size using linear discriminant analysis.

Figure-6 shows the supervised classified image using the linear discriminant function for the 40-training set size. By comparing with Table-3, it is clear that paddy region (yellow) is the largest (1595 m^2) occupying 45% of the image while banana region is the smallest (114 m^2) occupying 3% of the image.

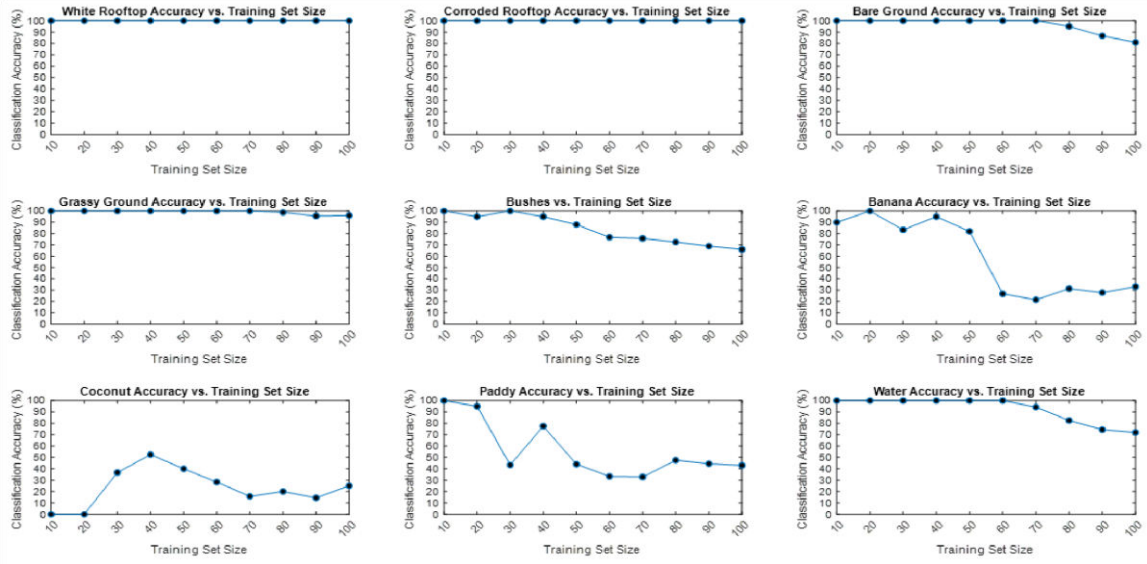

Figure-5. Individual class classification accuracy (producer accuracy) versus training set size for classified images using linear discriminant function.

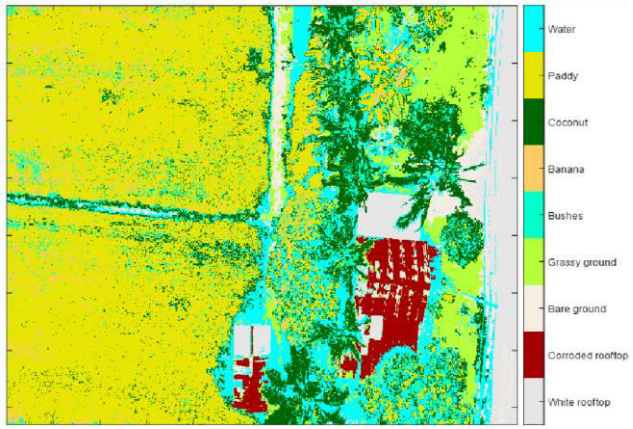

Figure-6. Supervised classified image using linear discriminant analysis.

Table-2. Class with pixel count, pixel percentage of the area for classified image using linear discriminant function.

Class	Pixel (count)	Pixel (%)	Area (m^2)
White rooftop	1422400	7	255
Corroded rooftop	680310	3	122
Bare ground	759910	4	136
Grassy ground	1577300	8	283
Bushes	1179200	6	212
Banana	636030	3	114
Coconut	2768400	14	497
Paddy	8882200	45	1595
Water	2056100	10	369
Total Classified Pixels	19962000	100	3584

Classification using Quadratic Discriminant Function

For the supervised classification using quadratic discriminant analysis (Figure-7), there is a gradual increase in overall accuracy from 10 to 40 training set size and then somewhat a decreasing trend from 40 to 100 training set size. The highest accuracy is at 40 training set size with 78.61% overall accuracy and 0.7594 Kappa Coefficient. Figure-8 shows individual class accuracy versus training set size for classified image produced based on quadratic discriminant function. Corroded rooftop and bare ground overall have the highest and most stable trend as the number of training set size increases. White rooftop and grassy ground show an increasing trend as training set size increases. Coconut and paddy have somewhat a fluctuating trend.

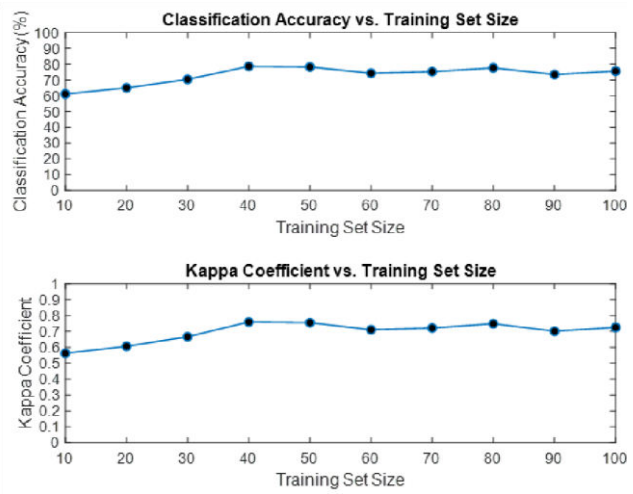

Figure-7. Overall classification accuracy and Kappa coefficient versus training set size using quadratic discriminant analysis.

Figure-9 shows the supervised classified image using quadratic discriminant function. Like linear discriminant function, it is obvious that paddy (yellow) possesses the most pixels within the image occupying 1570 m^2, covering 44% of the image as shown in Table V. Compared to linear discriminant function that classifies banana as the class with least pixels, the quadratic discriminant function the least pixels are possessed by corroded rooftop (brown) occupying 117 m^2 covering 3% of the image.

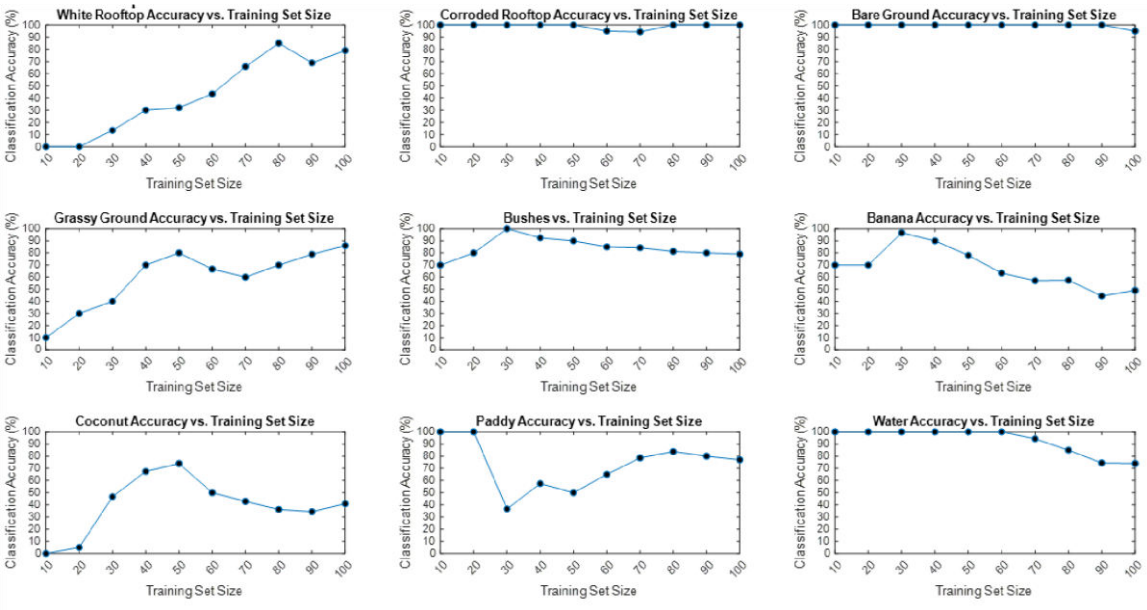

Figure-8. Individual class classification accuracy (producer accuracy) versus training set size for the classified images that are based on quadratic discriminant function.

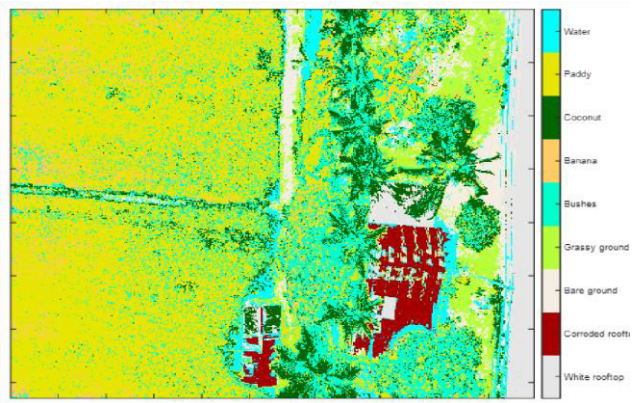

Figure-9. Supervised classified image using quadratic discriminant function.

Table-3. Class with pixel count, pixel percentage of the area for classified image using quadratic discriminant function.

Class	Pixel (count)	Pixel (%)	Area (m^2)
White rooftop	1150400	6	207
Corroded rooftop	653430	3	117
Bare ground	1024700	5	184
Grassy ground	1328900	7	239
Bushes	3401700	17	611
Banana	805770	4	145
Coconut	1882100	9	338
Paddy	8743100	44	1570
Water	971780	5	174
Total Classified Pixels	19962000	100	3584

Classification using Diagonal Linear Discriminant Function

For the supervised classification using diagonal linear discriminant function (Figure-10), there is a decrease trend in overall accuracy from 10 to 30 training set size and then somewhat a constant trend from 30 to 100 training set size. The highest accuracy is at 10 training set size with 82.22% overall accuracy and 0.8 Kappa Coefficient. Figure-11 shows individual class accuracy

versus training set size for classified image produced based on quadratic discriminant function. White and corroded rooftop overall have the highest and most stable trend as the number of training set size increases. Banana and water show a decreasing trend as training set size increases. Coconut and paddy have somewhat a fluctuating trend.

Figure-12 shows the supervised classified image using diagonal linear discriminant function. Like linear and quadratic, it is obvious that paddy (yellow) possesses the most pixels within the image occupying 1519 m^2, covering 42% of the image as shown in Table-5. The least pixels are possessed by white rooftop (white) occupying 86 m^2 covering 2% of the image.

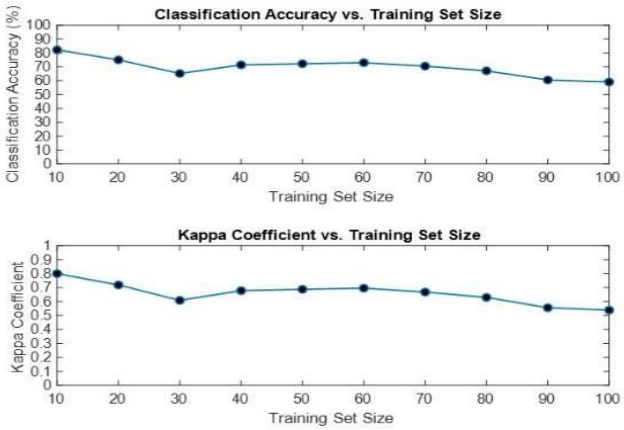

Figure-10. Overall classification accuracy and Kappa coefficient versus training set size using diagonal linear discriminant function.

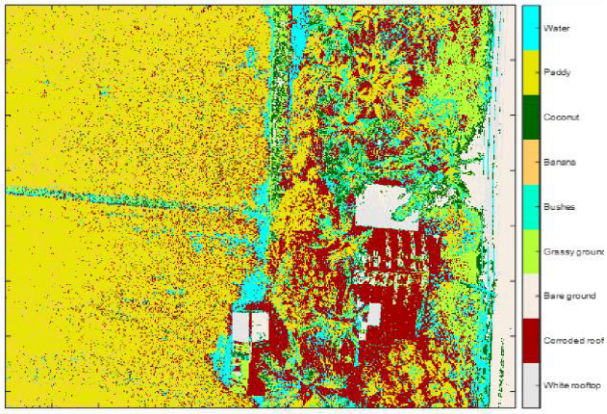

Figure-11. Supervised classified image using diagonal linear discriminant function.

Table-4. Class with pixel count, pixel percentage of the area for classified image using diagonal linear discriminant function.

Class	Pixel (count)	Pixel (%)	Area (m^2)
White rooftop	477060	2	86
Corroded rooftop	3662000	18	658
Bare ground	1171300	6	210
Grassy ground	1357200	7	244
Bushes	487400	2	88
Banana	1910500	10	343
Coconut	1001900	5	180
Paddy	8459400	42	1519
Water	1434900	7	258
Total Classified Pixels	19962000	100	3584

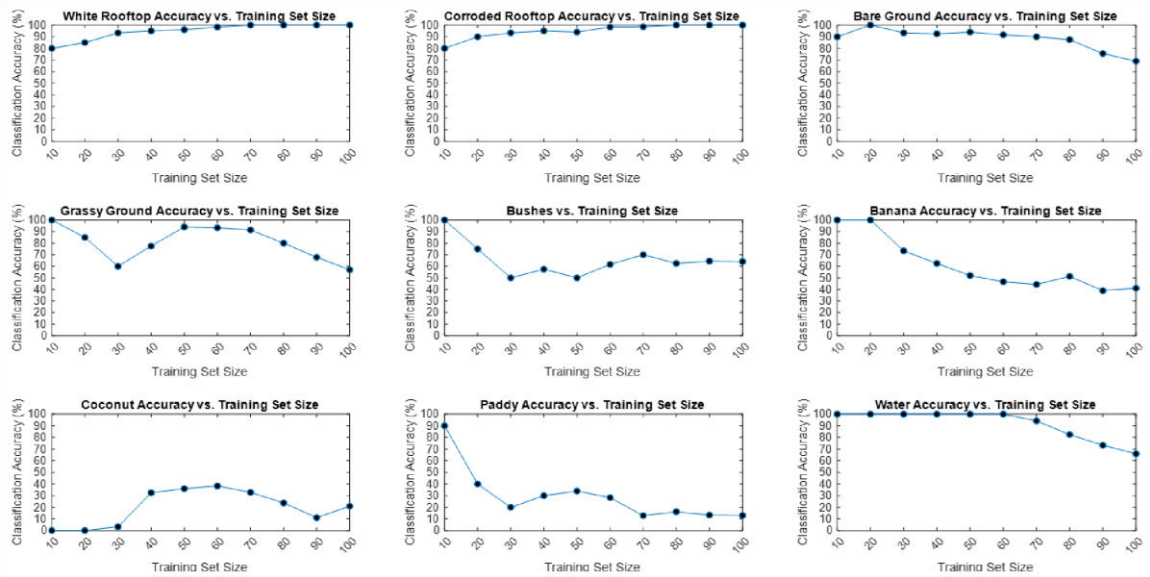

Figure-12. Individual class classification accuracy (producer accuracy) versus training set size for classified images using diagonal linear discriminant function.

Classification using Diagonal Quadratic Discriminant Function

For the supervised classification using diagonal quadratic discriminant function (Figure-13), there is a decreasing trend in overall accuracy from 10 to 30 training set size and then a steadily increasing trend from 30 to 50 training set size before showing somewhat a constant towards 100 training set size. The highest accuracy is at 10 training set size with 73.33% overall accuracy and 0.7 Kappa Coefficient. Figure-14 shows individual class accuracy versus training set size for classified image produced based on quadratic discriminant function. White rooftop and bare ground have overall the highest and most stable trend as the number of training set size increases. Banana and bushes show a decreasing trend as training set size increases. Coconut and paddy have somewhat a fluctuating trend.

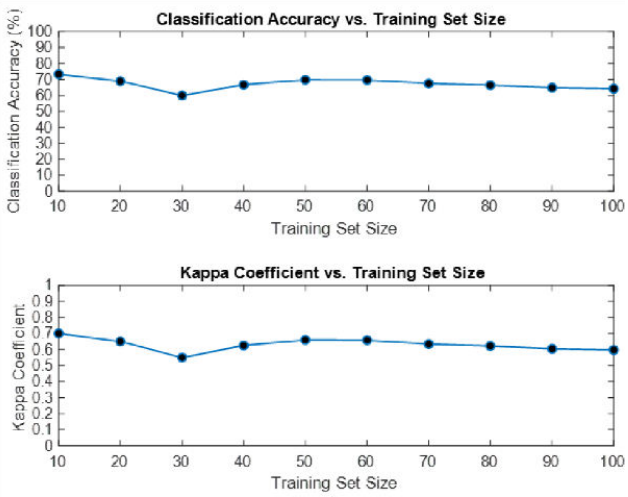

Figure-13. Overall classification accuracy and Kappa coefficient versus training set size using diagonal quadratic discriminant function.

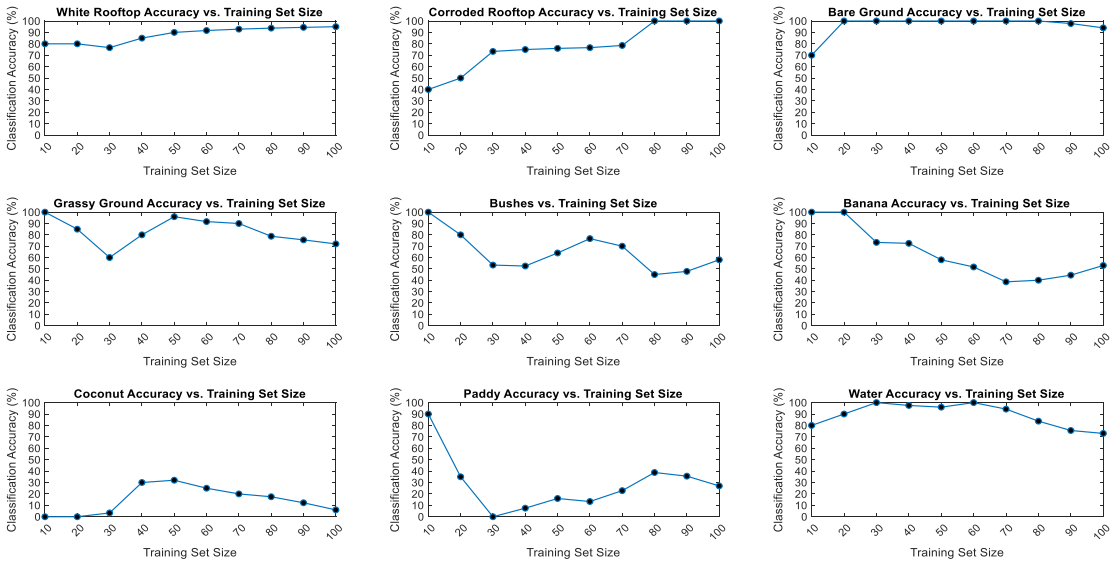

Figure-14. Individual class classification accuracy (producer accuracy) versus training set size for classified images using diagonal quadratic discriminant function.

Figure-15 shows the supervised classified image using diagonal quadratic discriminant function. It is obvious that paddy (yellow) possesses the most pixels within the image occupying 2498 m^2, covering 70% of the image as shown in Table IX. The least pixels are possessed by water occupying 40 m^2 or 1% of the image.

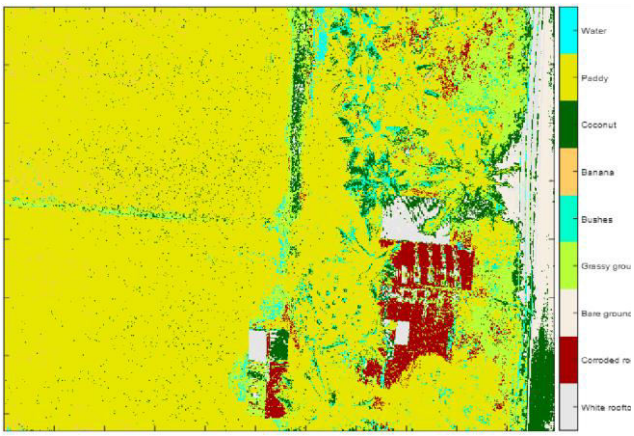

Figure-15. Supervised classified image using diagonal quadratic discriminant function.

Figure-16 shows overall accuracy, Kappa Coefficient, training set size and time for the classifications that are based on linear, quadratic, diagonal linear and diagonal quadratic discriminant function respectively. Linear discriminant function has the highest overall classification accuracy and Kappa Coefficient of 91% and 0.9 respectively followed by diagonal linear discriminant function (82% overall accuracy and 0.8 Kappa Coefficient), quadratic discriminant function (79% overall accuracy and 0.76 Kappa Coefficient) and diagonal quadratic discriminant function (73% overall accuracy and 0.7 Kappa Coefficient). For the optimal training set size, linear and quadratic discriminant function use 40- while diagonal linear and quadratic discriminant function use 10- training set size. In term of time, diagonal quadratic has the fastest processing time (572 s) followed by linear (640 s), quadratic (670 s) and diagonal linear (682).

Table-5. Class with pixel count, pixel percentage of the area for classified image using diagonal quadratic discriminant function.

Class	Pixel (count)	Pixel (%)	Area (m^2)
White rooftop	484450	2	87
Corroded rooftop	824170	4	148
Bare ground	767990	4	138
Grassy ground	1772100	9	318
Bushes	402230	2	72
Banana	254470	1	46
Coconut	1319500	7	237
Paddy	13913000	70	2498
Water	224040	1	40
Total Classified Pixels	19962000	100	3584

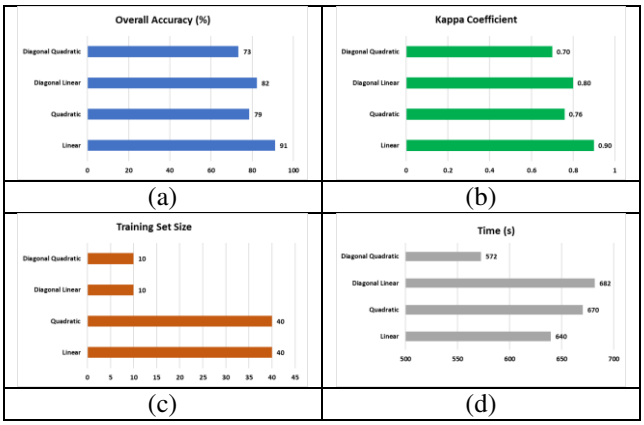

Figure-16. (a) Overall accuracy, (b) Kappa Coefficient, (c) training set size and (d) time for linear, quadratic, diagonal linear and diagonal quadratic discriminant function.

Figure-17 shows the percentage of correctly classified pixels for white rooftop, corroded rooftop, bare ground, grassy ground, bushes, banana, coconut, paddy and water. For White rooftop, linear (100%) and quadratic (30%) discriminant function give the highest and lowest accuracy respectively. For corroded rooftop and bare ground, linear and quadratic are the highest (100%) while diagonal quadratic is the lowest (40% and 70% for corroded rooftop and bare ground respectively). For grassy ground, quadratic is the lowest (70%) while 100% for the rest. For banana, bushes and paddy, diagonal linear and diagonal quadratic are the highest (100% for banana and bushes while 90% for paddy) while quadratic is the lowest (90%, 92.5% and 57.5%) for banana, bushes and paddy respectively). For coconut, the highest is quadratic (67.5%) while 0% for diagonal linear and diagonal quadratic. For water, all discriminant functions have 100% accuracy except diagonal quadratic discriminant function (80%).

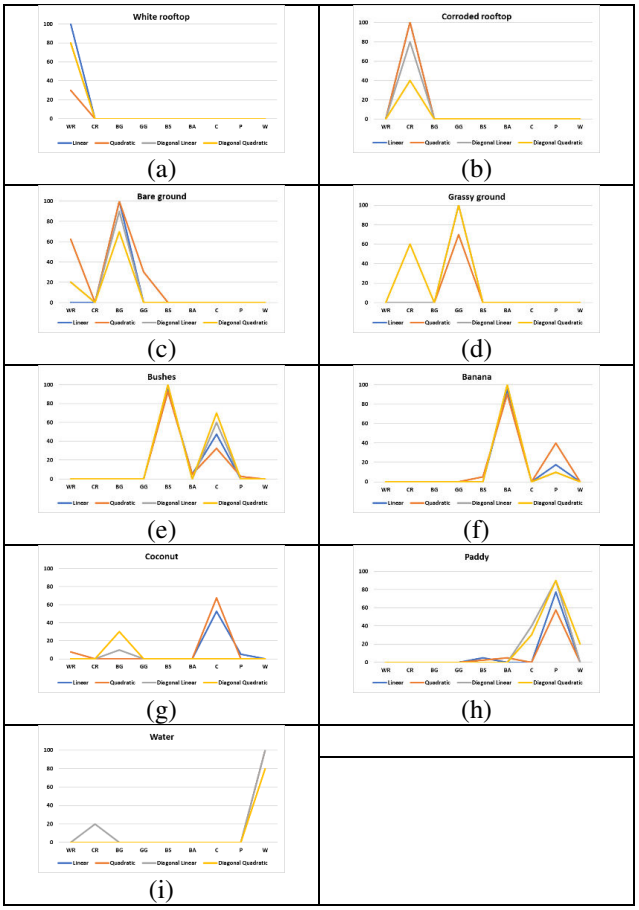

Figure-17. Percentage of correctly classified pixels based on linear, quadratic, diagonal linear and diagonal quadratic discriminant function.

Figure-18 shows area percentage versus class for the classifications that are based on linear, quadratic, diagonal linear and diagonal quadratic discriminant function. It can be seen that all discriminant functions give paddy as the dominant object in which among them, the largest area is given by diagonal quadratic discriminant

function. For corroded rooftop, diagonal linear discriminant function gives the largest area, while the rest of the discriminant functions have about the same size. For bushes, quadratic discriminant function has the largest area followed by linear, diagonal linear and diagonal quadratic discriminant function. For banana, diagonal linear discriminant function has the largest area followed by quadratic, linear and diagonal quadratic discriminant function. For coconut, linear discriminant function has the largest area followed by quadratic, diagonal quadratic and diagonal linear discriminant function. For water, linear discriminant function has the largest area followed by diagonal linear, quadratic and diagonal quadratic discriminant function. For white rooftop, linear discriminant function has the largest area followed by quadratic and the rest of discriminant functions. Grassy ground has about the same area for all discriminant functions.

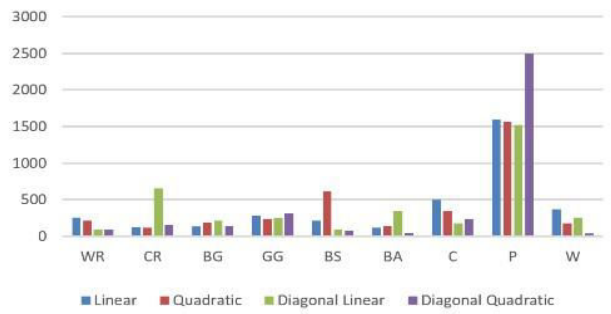

Figure-18. Area percentage versus class for the classification based on linear, quadratic, diagonal linear and diagonal quadratic discriminant function.

CONCLUSIONS

In this study, we have compared four types of discriminant functions namely linear, quadratic, diagonal linear and diagonal quadratic discriminant functions. Initially, K-means clustering of 9 clusters has been used in assisting the selection of training pixels for the supervised classification. The classification has been experimented for training set size 10 through 100 for linear, quadratic, diagonal linear and diagonal quadratic discriminant function. From, the classification outcomes, training set size 40 and 10 has been identified to be the optimal training set sizes for linear and quadratic, and diagonal linear and quadratic respectively due to having the highest overall classification accuracy and Kappa coefficient for the respective discriminant functions. Overall, the linear discriminant function has been found to produce the highest overall accuracy and having more realistic class area percentages of the study area compared to the quadratic, diagonal linear and diagonal quadratic discriminant function. Nevertheless, the performance of supervised classification is greatly influenced by the way the sampling of the training pixels is made with respect to the discriminant functions used in which is not investigated in-depth in this study. Therefore, future work will take into consideration investigating the effects of different patterns of systematic sampling of training pixels on classification performance by taking into account the particular technique used.

ACKNOWLEDGEMENTS

The authors would like to thank the Malaysian Ministry of Higher Education (MOHE) for funding this research through the Prototype Research Grant Scheme (PRGS) (PRGS/1/2021/ICT07/UTEM/02/1) and Universiti Teknikal Malaysia Melaka (UTeM) for all the support throughout this research Scheme.

REFERENCES

[1] Gerten D., V. Heck and J. Jägermeyr. 2020. Feeding ten billion people is possible within four terrestrial planetary boundaries. Nature Sustain. 3: 200-208.

[2] Subramaniam M., R. Yogambigai and R. Khalid. 2017. Estimation of future Paddy Production and Sustainable Land Allocation in Malaysia: A Polynomial Approach. Pertanika Journal of Social Science and Humanities. 25. 1613-1624.

[3] Fellmann T., Witzke P., Weiss. 2018. Major challenges of integrating agriculture into climate change mitigation policy frameworks. Mitig Adapt Strateg Glob Change. 23, 451-468.

[4] Khazanah Research Institute. 2019. The Status of the Paddy and Rice Industry in Malaysia, Khazanah Research Institute, Kuala Lumpur, Malaysia.

[5] Ahmad A., H. Sakidin, A. Dahlia, Zetriuslita, R. Qudsi. 2020. Haze and its impact to paddy monitoring from remote sensing satellites, International Journal of Advanced Trends in Computer Science and Engineering. 9(4), 107: 4939-4946.

[6] Ahmad A., H. Sakidin, M. Y. A. Sari, A.R.M. Amin, S.F. Sufahani, A.W. Rasib. 2021. Naïve Bayes Classification of High-Resolution Aerial Imagery. (IJACSA) International Journal of Advanced Computer Science and Applications. 12(11): 168-177.

[7] Ahmad A., U. K. M. Hashim, R. Abd Wahid, H. Sakidin, S. F. Sufahani, A. R. M. Amin, M. M. Abdullah and S. Quegan. 2019. Implementation of land cover change detection based on supervised classifications of multispectral satellite data for leveraging the Internet of Things. ARPN Journal of Engineering and Applied Sciences. 14(10): 1863-1870.

[8] Lan Y., Z. Huang, X. Deng, Z. Zhu, H. Huang, Z. Zheng, B. Lian, G. Zeng and Z. Tong. 2020. Comparison of machine learning methods for citrus greening detection on UAV multispectral images.Computers and Electronics in Agriculture. 171: 1-11.

[9] Said M., M. Hany, M. Magdy, O. Saleh, M. Sayed, Y. M. I. Hassan and A. Nabil. 2021. Automated labeling of hyperspectral images for oil spills classification. International Journal of Advanced Computer Science and Applications (IJACSA). 12(8): 490-496.

[10] Rahmani M. K. I., N. Pal and K. Arora. 2014. Clustering of Image Data Using K-Means and Fuzzy K-Means. International Journal of Advanced Computer Science and Applications (IJACSA). 5(7): 160-163.

[11] Yang M., H. Mei and D. Huang. 2017. An effective detection of satellite images via K-means clustering on hadoop system. International Journal of Innovative Computing, Information and Control. 13(3): 1037-1046.

[12] Dudoit S., J. Fridlyand and T. P. Speed. 2002. Comparison of Discrimination Methods for the Classification of Tumors Using Gene Expression Data. Journal of the American Statistical Association. 97(457): 77-87.

[13] D. Park. 2016. Image classification using Naïve Bayes classifier. International Journal of Computer Science and Electronics Engineering (IJCSEE). 4(3): 135-139.

[14] Ho Y., Y. Huang, H. Chu and L. Chen. 2018. Adaptive sensing scheme using naive Bayes classification for environment monitoring with drone. International Journal of Distributed Sensor Networks. 14: 1-12.

[15] Schowengerdt R. A.2007. Remote sensing, models, and methods for image processing, 3rd ed., Academic Press: USA.

[16] Ahmad A. and S. Quegan. 2012. Analysis of maximum likelihood, classification on multispectral data. Applied Mathematical Sciences. 6(129): 6425-6436.

[17] YazidA., R. A. Wahid, K. M. Nazrin, A. Ahmad, A. S. Nasruddin, D. Rozilawati, M. A. Hamzah and M. Razak. 2019. Terrain mapping from unmanned aerial Vehicle. Journal of Advanced Manufacturing Technology. 13(1): 1-16.

[18] Ahmad A., K. A. M. Fauzey, M. M. Abdullah, S. F. Sufahani, M. Y. A. Sari and A. R. M. Amin. 2020. Noise and restoration of UAV remote sensing images. International Journal of Advanced Computer Science and Applications (IJACSA). 11(12): 175-183.

[19] Ahmad A. and S., Quegan. 2014. The effects of haze on the spectral and statistical properties of land cover classification. Applied Mathematical Sciences. 8(180): 9001-9013.

[20] Ahmad A., M. K. A. Ghani, S. Razali, H. Sakidin and N. M. Hashim. 2014. Haze reduction from remotely sensed data. Applied Mathematical Sciences. 8(36): 1755-1762.

[21] Ahmad A. and S. Quegan. 2015. The effects of haze on the accuracy of satellite land cover classification. Applied Mathematical Sciences. 9(49): 2433-2443.

[22] Sari N. A., A. Ahmad, M. Y. A. Sari, S. Sahib and A. W. Rasib. 2015. Development of rapid low-cost LARS platform for oil palm plantation. Jurnal Teknologi. 77(20): 99-105.

[23] Mahmood F., K. Abbas, A. Raza, M. A. Khan and P. W. Khan. 2019. Three-dimensional agricultural land modeling using Unmanned Aerial System (UAS). International Journal of Advanced Computer Science and Applications (IJACSA). 10(1): 443-449.

[24] Din N. U., B. Naz, S. Zai B. and W. Ahmed. 2021. Onion crop monitoring with multispectral imagery using deep neural network. International Journal of Advanced Computer Science and Applications (IJACSA). 12(5): 303-309.

[25] Sari M. Y. A., A. W. Rasib, H. M. Ali, A. R. M. Yusoff, M. I. Hassan, K. M. Idris, A. Ahmad and R. Dollah. 2018. 3D mapping based-on integration of uav platform and ground surveying. International Journal of Advanced Computer Science and Applications (IJACSA). 9(12): 160-168.

[26] Campbell J. B. 2002. Introduction to remote sensing. London: Taylor & Francis.

[27] Stehman S. V. 1997. Selecting and interpreting measures of thematic classification accuracy. Remote Sensing of Environment. 62: 77-89.

[28] Miguel-Ayanz S. J. and G. S. Biging. 1996. An iterative classification approach for mapping natural resources from satellite imagery. International Journal of Remote Sensing. 17: 957-982.

[29] Congalton R. G. 1991. A review of assessing the accuracy of classification of remotely sensed data. Remote Sensing of Environment. 37: 35-46.

[30] Lillesand T. M., R. W. Kiefer and J. W. Chipman. 2015. Remote Sensing and Image Interpretation. 7th Ed. NJ, USA: John Wiley & Sons.

[31] Koukoulas S. and G. A. Blackburn. 2001. Introducing new indices for accuracy evaluation of classified images representing semi-natural woodland environments. Photogrammetric Engineering and Remote Sensing. 67(4): 499-510.

[32] Thomlinson J. R., P. V. Bolstad and W. B. Cohen. 1999. Coordinating methodologies for scaling landcover classifications from site-specific to global: steps toward validating global map products. Remote Sensing of Environment. 70: 16-28.

[33] Ahmad A. and S. Quegan. 2014. Multitemporal cloud detection and masking using MODIS data. Applied Mathematical Sciences. 8(7): 345-353.

[34] Wulder M. A., S. E. Franklin, J. C. White, J. Linke and S. Magnussen. 2006. An accuracy assessment framework for large-area land cover classification products derived from medium-resolution satellite data. International Journal of Remote Sensing. 27: 663-683.

[35] Ahmad A. and S. Quegan. 2014. Haze modelling and simulation in remote sensing satellite data. Applied Mathematical Sciences. 8(159): 7909-7921.

[36] Hayat M. A., J. Wu and Y. Cao. 2020. Unsupervised Bayesian learning for rice panicle segmentation with UAV images. Plant Methods. 16(18): 1-13.

[37] Rosle R., N. Sulaiman, N. N. Che'Ya, M. F. M Radzi, M. H. Omar, Z. Berahim, W. F. F Ilahi, J. A. Shah and M. R. Ismail. 2022. Weed detection in rice fields using UAV and multispectral aerial imagery. Chem. Proc. 10(44): 1-11.